2023-12-01

Study Of Human Circadian Protein (hRORy) And Lipid-Protein Interaction In Giant Virus (pbcv-1)

Laila Noor
University of Texas at El Paso

STUDY OF HUMAN CIRCADIAN PROTEIN (hRORγ) AND LIPID-PROTEIN INTERACTION IN GIANT VIRUS (PBCV-1)

LAILA NOOR

Master's Program in Chemistry

APPROVED:

Chuan (River) Xiao, Ph.D., Chair

Mahesh Narayan, Ph.D.

Lin Li, Ph.D.

Amol Kulkarni, Ph.D.

Stephen L. Crites, Jr., Ph.D.
Dean of the Graduate School

Dedication

I intend to devote my master's thesis to my parents, acknowledging their unwavering encouragement, tireless efforts, and for instilling in me the aspiration for advanced education from my earliest years. Their unwavering support, nurturing, and blessings led to this milestone. I hold them in perpetual appreciation for everything they've done.

STUDY OF HUMAN CIRCADIAN PROTEIN (hRORγ) AND LIPID-PROTEIN INTERACTION IN GIANT VIRUS (PBCV-1)

by

LAILA NOOR

THESIS

Presented to the Faculty of the Graduate School of

The University of Texas at El Paso

in Partial Fulfillment

of the Requirements

for the Degree of

MASTER OF SCIENCE

Department of Chemistry and Biochemistry

THE UNIVERSITY OF TEXAS AT EL PASO

December 2023

Acknowledgments

I am grateful to the Department of Chemistry and Biochemistry at the University of Texas at El Paso (UTEP) for their support throughout my studies. I want to convey my gratitude to my mentor, Dr. Chuan (River) Xiao, a Professor in the Department of Chemistry and Biochemistry, for his constant encouragement and guidance. Dr. Xiao's dedication and time spent on this project have been invaluable to my research success.

I am also grateful to my committee members, Dr. Chuan Xiao, Dr. Mahesh Narayan, Dr. Lin Li, and Dr. Amol Kulkarni, for their essential expertise and contributions to the success of my studies. I am deeply thankful to the Department of Chemistry and Biochemistry at UTEP for providing me with a teaching assistant position and their assistance throughout my studies. I would like to express my gratitude to Dr. James L. Van Etten, Professor at the University of Nebraska-Lincoln, for providing the PBCV-1 virus samples. I also want to extend my gratitude to Dr. Daniel Capelluto, an Associate Professor of Biological Science at Virginia Tech, for collaborating with us on the PBCV-1 project. My learning experience has been enriched by both former and current lab members, and I am grateful for their assistance. I want to offer special thanks to Sebastian Sanchez and Yuejiao Xian for their contributions to the hRORγ project.

My family, friends, and husband have been unwavering in their support throughout my journey. Their encouraging words and backing were vital in helping me achieve my goals. I cannot forget to express my deepest appreciation to them.

As I look back on my graduate school experience with fondness, I am excited for the future that lies ahead. I greatly appreciate everyone mentioned above for being an integral part of my journey and crafting it into an unforgettable experience.

Abstract

Project 1: Circadian rhythm is a 24-hour cycle that regulates physical and behavioral changes such as sleep-wake patterns in humans, tailoring the daily light and dark changes. Long-term disruption in circadian rhythms can cause sleep disorders such as sleep apnea, insomnia, et al. Limited research has been done on potential drugs to treat against circadian related sleep disorders. Inside the cell at molecular level, the circadian rhythm is regulated by interlocked time-delayed feedback loops, which involve positive and negative transcriptional regulators. Experimental results showed transcriptional factors Retinoic Acid Receptor-Related Orphan Receptors (RORs) improve the stability and functionality of the circadian rhythm. Nobiletin is a natural flavonoid that has been reported to enhance the circadian amplitude by binding to human ROR gamma (hRORγ) with high affinity. However, the molecular interaction between Nobiletin and hRORγ remains unknown, which limits the future application of Nobiletin as a potential circadian interfering medicine to treat related diseases. The final goal of the project is to determine the atomic three-dimensional structure of the hRORγ/Nobiletin complex, with a focus on comprehending their interaction. The hRORγ gene was cloned and expressed in bacteria to obtain substantial quantities of purified recombinant hRORγ. The expression and purification protocols have been intensively optimized. The affinity tag has been removed by enzymatic digestion, providing homogenous charge-neutral recombinant hRORγ to be ready to co-crystalized with Nobiletin for atomic structural determination by X-ray crystallography. The resultant structure will illustrate the mechanism of Nobiletin's impact on circadian rhythm, paving the way for potential drug development.

Project 2: Giant viruses are characterized by their remarkable size, complex genetic content, and unique replication mechanisms. Most giant viruses have icosahedral shell called capsid assembled mainly from the major capsid proteins (MCPs). Closely beneath this MCP layer is a lipid membrane. The goal of the project is to study the interaction between MCP and lipid using the giant virus Paramecium bursaria chlorella virus 1 (PBCV-1). By employing mass spectrometry (MS) analyses and the following lipidomic analyses, various lipids have been identified within the virion. To investigate the specific interaction between MCP and lipids, Viral protein 54 (Vp54), the MCP of PBCV-1, was purified through multiple steps, allowing for an in-depth study of its affinity to lipids. The following liposome pull-down assay revealed Vp54 specifically binds to cardiolipin, a lipid found in mitochondria. This research contributes to the broader knowledge of the mechanisms underlying giant virus assembly, shedding light on the critical role of lipid-protein interactions in this process.

Table of Contents

List of Tables

List of Figures

List of Illustrations

Chapter 1: Expression and purification of human circadian protein hRORγ for potential drug target studies

1.1. INTRODUCTION

Life is a complex and cyclical chemical process that operates in four dimensions. It encompasses a journey from a single cell to full-fledged adulthood, followed by the inevitable changes from adulthood to death. This highlights the fact that life is indeed a cycle, containing numerous smaller cycles, such as seasonal, monthly, half-monthly, and daily cycles [1]. Numerous life forms on our planet have developed internal biological clocks that harmonize with the natural cycle of the sun's ascent and descent. These clocks, known as circadian clocks, operate on a 24-hour cycle and assist organisms in anticipating and adapting to the routine fluctuations in their surroundings throughout the day. The circadian clocks regulate various aspects of an organism, including biochemical reactions, bodily processes, and behaviors, ensuring they are in sync with the daily alternation of light and darkness [2]. In 1729, Jean Jacques d'Ortous de Mairan observed the first circadian rhythm in a mimosa plant, revealing an internal biological timing system [3, 4]. German biologist Erwin Bünning later studied plant circadian rhythms, finding that they have a 24.4-hour cycle and can be inherited, showing the presence of an internal clock synchronized by external cues [5]. In the 1970s and 1980s, significant advances in DNA technology allowed for the cloning and study of the Drosophila Period gene by Michael Rosbash, Jeffrey C. Hall, and Michael W. Young [6, 7]. Independently, they accomplished substantial contributions to the field of circadian rhythm resulting in their winning the 2017 Nobel Prize in Medicine. Following this discovery, many circadian genes were discovered and investigated [8, 9]. To explain how the

circadian rhythm functions, researchers proposed a biological mechanism referred as transcriptional-translational feedback loop (TTFL) (Figure 1) [10, 11].

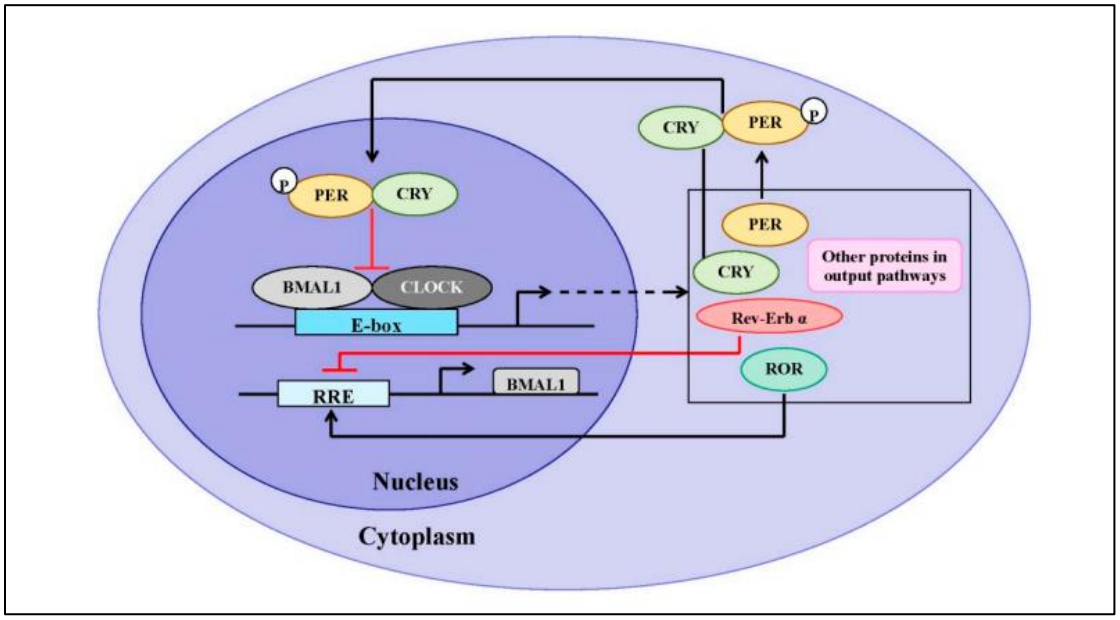

Figure 1: The schematic diagram of TTFL in circadian rhythm. (adapted from Wang, C., et al., 2014 [12]).

Inside the mammals, the TTFL is a fundamental mechanism of circadian rhythm where the transcription and translation of specific genes, such as those encoding circadian clock proteins, creating a feedback loop that drives the rhythmic regulation of biological processes. The TTFL composes of a group of transcriptional factors. Among these factors are Circadian Locomotor Output Cycles Kaput (CLOCK) and Brain and Muscle Arnt-Like 1 (BMAL1). CLOCK and BMAL1 form a pair of essential circadian proteins, heterodimerizing into a transcriptional activator complex that regulates circadian rhythms and gene expression in living organisms [13]. By bonding to E-Box DNA elements, the CLOCK/BMAL1 complex begins the transcription of several genes related to the circadian rhythm, such as Period (Per) and Cryptochrome (Cry). As Per and Cry mRNAs translate into proteins in the cytosol, it leads to the accumulations of PER/CRY complexes [12, 14]. After a delay to reach a concentration threshold, the PER/CRY

complexes translocate into the nucleus to negatively regulate CLOCK/BMAL1 functions, leading to the inhibition of Per and Cry transcriptions. In nocturnal mammals, the PER/CRY complexes are inhibited throughout the night until they are sufficiently broken down by a ubiquitin-proteasome system [15, 16]. The TTFL sustains this cycle with a periodicity of approximately 24 hours. Every cell in multicellular animals has its own TTFL-controlled circadian rhythm that needs to be coordinated at the body level. Mammals' central timepiece is found in the hypothalamic suprachiasmatic nucleus (SCN). This main pacemaker controls and synchronizes peripheral clocks with the input of zeitgebers (external cues, such as light and social activities)[15, 17, 18]. Light serves as the master clock's primary zeitgeber. The SCN uses neurotransmitters to synchronize the circadian rhythms of peripheral cells in response to light signals [17].

1.1.1. Nuclear Receptors

Circadian rhythm uses ligand-regulated transcriptional factors known as nuclear receptors (NRs) that play a crucial role in regulating metabolism, development, and immunity. NRs are a class of drug targets for treating various human disease [19, 20]. The NRs facilitate the binding of extracellular signaling molecules to specific DNA sequences, thus enabling the regulation of transcriptional responses [21]. The NR superfamily includes Retinoic acid receptor-related orphan receptors (RORs) and nuclear receptor subfamily 1 group D (Rev-Erb), which are essential in regulating the circadian clock's activity. The ROR and Rev-Erb regulate TTFL loop activity by controlling BMAL1 expression and stabilizing the feedback loop [15, 22]. RORs positively regulate BMAL1 expression and sustain a proper circadian rhythm. In contrast, Rev-Erb negatively regulates BMAL1 expression (Figure 1) [23]. This thesis focuses on RORs that improve circadian rhythm stability and functionality [21].

1.1.2. The retinoic acid-related orphan receptors (RORs)

The ROR family is comprised of three receptors: RORα, RORβ, and RORγ [21, 24, 25]. RORα was first discovered in the early 1990s, followed by RORβ and RORγ. These RORs have sequence similarities to the retinoic acid receptor (RAR) and the retinoid X receptor (RXR) [15, 21, 25]. Structurally, RORs contain four major functional domains, which are an N-terminal (A/B) domain, a highly conserved DNA-binding domain (DBD), a hinge domain, and a C-terminal ligand-binding domain (LBD) (Figure 2)[21]. The LBD of RORs contains 12 α-helices and two additional extensions, H2' and H11'[26]. Among these, Helix 12 contains a PLYKELF sequence that is conserved amongst all the RORs and forms the activation function 2 (AF-2) (Figure 2) [21, 24]. Although the ligand binding pockets of all three ROR members have similar volume, the shape of RORγ's pocket is unique [26]. Depending on the type of ligand bound, RORs can interact with coactivators and corepressors, functioning as both transcriptional activators and repressors [27].

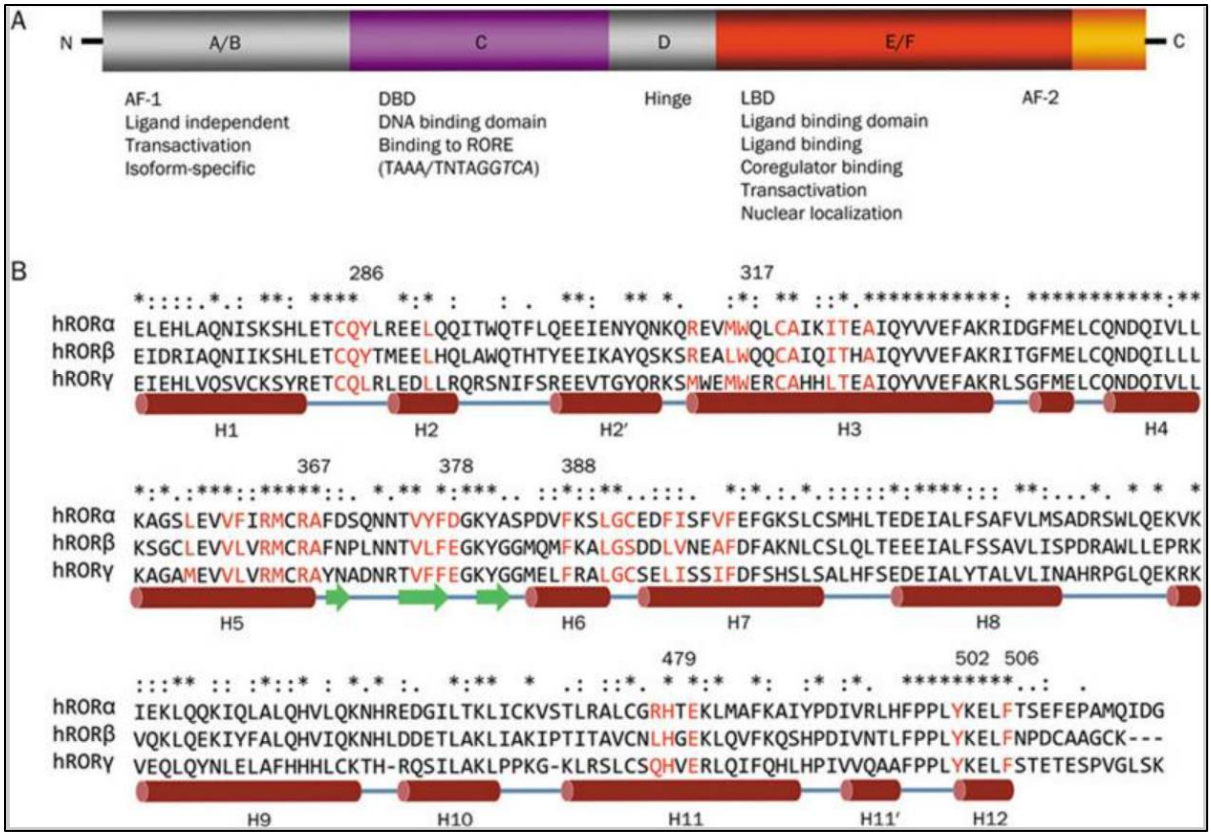

Figure 2: Domain structure and sequence alignment of RORs. (A) Schematic diagram of the domain structure of RORs contains activation function 1 (AF-1) region, followed by a DNA binding domain (DBD), a hinge domain, and a ligand-binding domain and an activation function 2 (AF-2) region. **(B)** Sequence alignment of the ligand binding domain of RORα, RORβ, and RORγ performed using ClustalW. The figure is adapted from Zhang, Y., et al., 2015 [21].

1.1.3. Pharmacological effects of nobiletin

Nobiletin, a flavonoid abundant in citrus fruits, has emerged as a compound of interest due to its potential pharmacological activities such as anti-cancer, anti-inflammatory, anti-allergy, anti-obesity, anti-diabetic, anti-microbial, antioxidant, and anti-neurodegenerative effects [28-30]. Moreover, the compound has a good safety profile. Its antioxidant properties improve heart health by reducing stress and controlling cholesterol levels. [31, 32]. Nobiletin also exhibits neuroprotective properties, offering promise in preventing neurodegenerative disorders. Additionally, Nobiletin has been explored for its anti-cancer potential and ability to protect the live (Figure 3)[33].

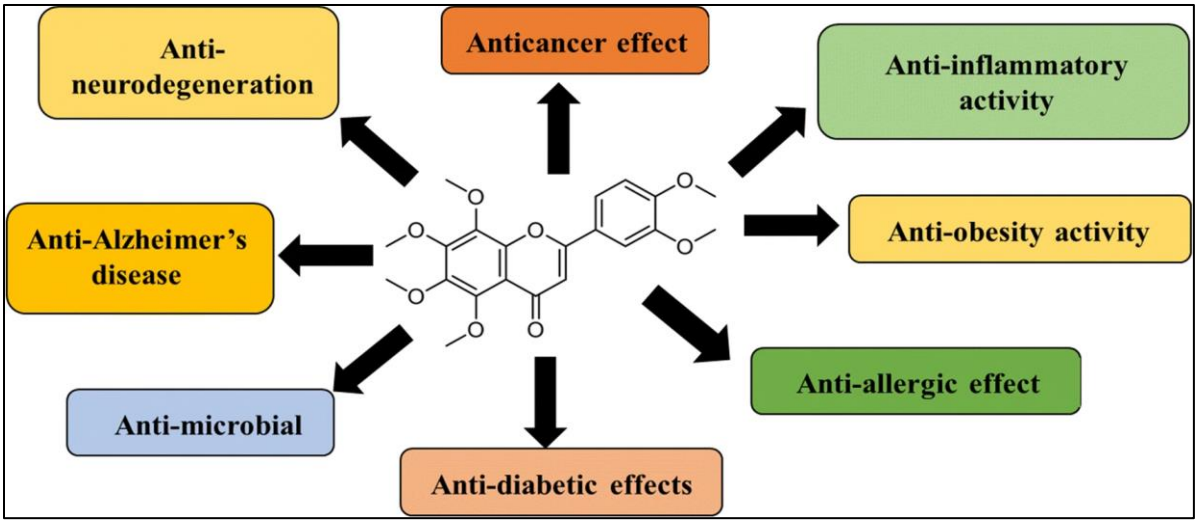

Figure 3: Pharmacological effects of Nobiletin (adapted from Kesharwani, S.S., et al., 2020 [33]).

1.1.4. Nobiletin targets the circadian oscillator to enhance clock protein activity

Scientists investigated the effects of Nobiletin as a modulator for enhancing clock function [34]. One study explored the possibility of metabolic protection by Nobiletin in obese mice. After 10-week treatment with Nobiletin, a significant decrease in body weight gain was observed in the wild-type obesity mice but not in the clock disrupted ones [35]. Previous studies have also revealed that 63% of Nobiletin-responsive genes showed promoter occupancy of core clock [36]. Further experiments were conducted to understand the effects of Nobiletin on the clock protein RORα. NOB dose-dependently increased Bmal1 promoter-driven luciferase reporter activity in Hepa1-6 cells that expressed wild-type RORα or RORγ [35]. This suggests that Nobiletin directly binds to and activates RORs (RORα and RORγ), and the presence of RORα/γ is necessary for the enhancing activity of Nobiletin on Bmal1 transcription [35].

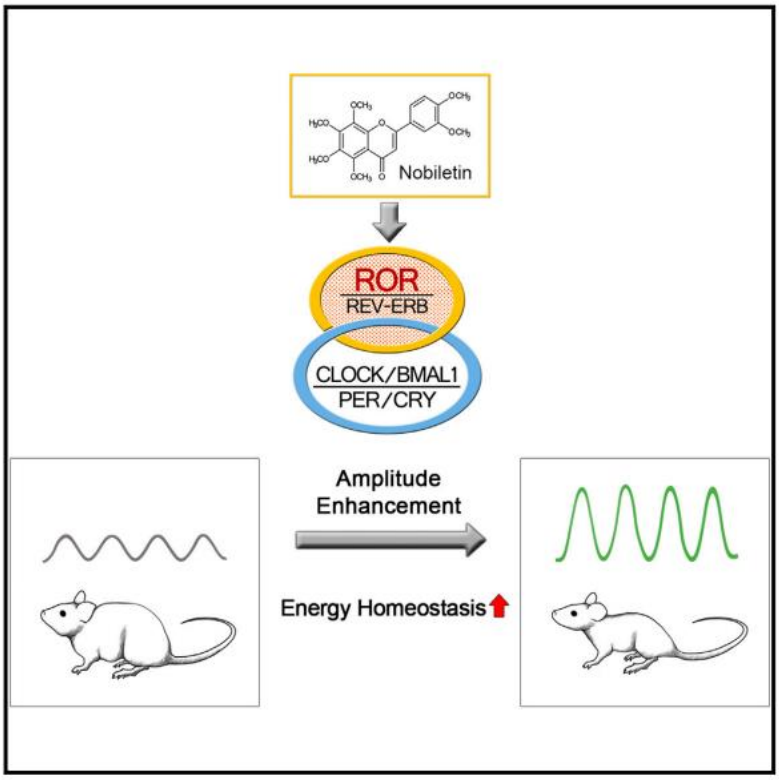

Figure 4: Nobiletin targets the circadian oscillator to enhance clock protein activity (adapted from He, B., et al., 2016 [35]).

1.1.5. Goal

The long-term goal of this project is to investigate how Nobiletin affects the activity of hRORγ and explore its mechanism as an enhancer of circadian rhythm. To achieve this, we want to determine the structure of hRORγ complex with Nobiletin. The expression vector for hRORγ was obtained from published result and transformed into bacterial cell. The recombinant hRORγ is expressed and purified to high concentration with homogeneity. This concentrated hRORγ protein will be co-crystallized with Nobiletin for structural determination using X-ray crystallography (Illustration 1). The resultant structure will shed light on the molecular interaction between hRORγ and Nobiletin. The findings of this study are expected to contribute to the understanding of the mechanism how Nobiletin enhance circadian rhythm. Ultimately, this

research could pave the way for developing new therapeutic treatment for circadian-related disorders.

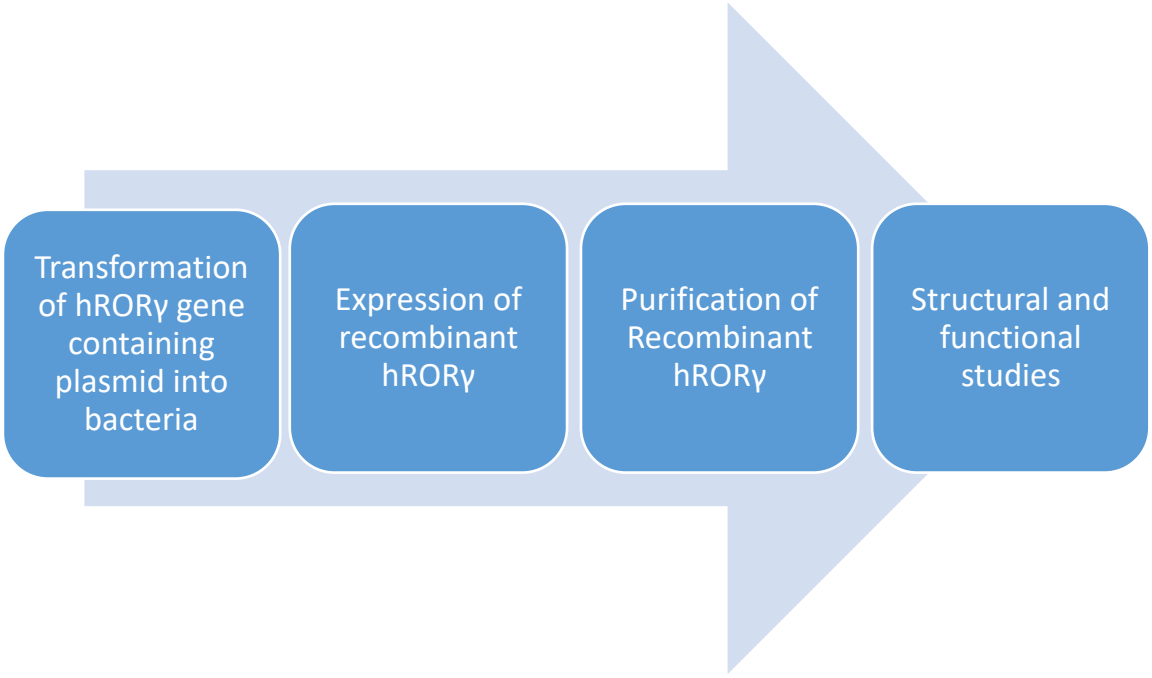

Illustration 1: Schematic diagram of experimental design

1.2. Materials and Methods

1.2.1. Glycerol stock preparation

The transformation of the pET46 plasmid incorporating the hRORγ gene into *E. Coli* Rosetta2 cells was carried out by Yuejiao Xian, a formal lab member who also prepared the original glycerol stock. To prepare the original glycerol stock, preculture was grown from the colony obtained from the transformation plate, using Terrific Broth (TB) media. The TB media was prepared by combining 47.6g of TB powder (Cat. no. BP97285), 4ml of glycerol, and 1000ml of distilled water, which was then autoclaved at 121°C for 30 minutes. After adding 0.5ml of preculture to 50ml of TB media, the culture was grown with ampicillin and chloramphenicol at the final concentration of 100µg/ml and 34µg/ml, respectively. When the optical density (OD_{600}) of

the culture reached 0.8, the original stocks were prepared with the final concentration of 15% glycerol and flash freeze using liquid nitrogen. To prepare a new glycerol stock for protein expression, a preculture was prepared from the original glycerol stock by pocking ice from it, monitored by overnight growth. 15% glycerol stocks were prepared using a similar method.

1.2.2. The large-scale expression of hRORγ

For the large-scale protein expression, a 50ml preculture was prepared using 50ml of TB media along with ampicillin and chloramphenicol to the final concentration of 100μg/ml and 34μg/ml, respectively. The preculture grew at 37°C with continuous shaking at 200rpm for 12 hours. After 12 hours of incubation, 4L TB cultures were prepared for the expression with same ampicillin and chloramphenicol and 10ml preculture was added to each culture. These cultures were then grown at 37°C with continuous shaking at 200rpm until OD_{600} reached 0.6. The temperature was reduced to 25°C in preparation for induction. Aliquots of 3ml of the culture were transferred into separate culture tubes and kept under the same conditions as an uninduced control. For induction, 1mM of final concentration of Isopropyl β-D-1-thiogalactopyranoside (IPTG) was added once the temperature reached the target level. The cultures were then allowed to express the protein for 6 hours at 25°C.

1.2.3. Cell harvesting and lysis

After the 6-hour expression period, the cell cultures were harvested by centrifugation at 4,690xg for 25 minutes. The resulting cell pellets were resuspended with Buffer A (20mM Tris-HCl, 500mM NaCl, 20mM imidazole, 10% glycerol, and pH 8.0) for hRORγ. For every 0.1g of pellet, 1ml of Buffer A was added. To facilitate cell lysis, lysozyme was added to the final concentration of 0.2mg/ml. The lysate was incubated at room temperature for 30 minutes. Finally, the protein lysate was stored at a temperature of -20°C. Prior to the purification, frozen lysate was

thawed and Phenylmethylsulfonyl fluoride (PMSF) was added to the final concentration of 10μM. The microfluidizer (Microfluidics, Model no. 110L) was further used with one passage to break the bacterial cell walls to release the recombinant protein. The sample was then incubated with DNase to the final concentration of 20μg/ml, for 20 minutes at room temperature. Cell debris was removed by centrifugation at 54,000xg and the supernatant was filtered through 0.2μm filters prior to affinity purification.

1.2.4. Affinity chromatography purification

AKTA FPLC (GE Healthcare) was used for affinity purification of recombinant hRORγ. A 5ml HisTrap HP affinity chromatography column (GE Cat. no. 17524802) was prepared and equilibrated with filtered and degassed Buffer A (20mM Tris–HCl, 500mM NaCl, 20mM imidazole, 10% glycerol, and pH 8.0). The supernatant samples were loaded onto the column at a flow rate of 1ml/min. The column was washed with Buffer A until the UV absorption stabilized at its lowest value. To ensure the removal of non-specific binding protein, 20 column volume of washing solution were applied to the column by mixing Buffer A with 8% Buffer B (20mM Tris–HCl, 500mM NaCl, 500mM imidazole, 10% glycerol, and pH 8.0) using AKTA FPLC system to reach final concentration of 60mM imidazole. Recombinant hRORγ was eluted with a solution at 200mM imidazole final concentration. Throughout the purification process, protein fractions were collected, and their purity were evaluated using sodium dodecyl sulfate-polyacrylamide gel electrophoresis (SDS-PAGE). Following the elution at 200mM imidazole, the eluted protein was immediately desalted using a 53mL HiPrep 26/10 desalting column (GE Cat. no. 17508701). The desalting column was equilibrated with filtered and degassed desalting buffer (50mM Tris-HCl, 200mM NaCl, 2mM DTT, and pH 8.0). This process effectively removes excess imidazole and

other small molecules from the protein sample. The concentration of the desalted protein was determined using Pierce Bradford Protein Assay kit (Thermo Fisher Scientific Cat. no. 23200).

1.2.5. Thrombin digestion and concentrating of hRORγ

To remove the his-tag of the recombinant protein, 100µl of the thrombin-agarose suspension 50% (v/v) (Sigma-Aldrich Cat. no. RECOMT) is added to 1ml of sample to cleave 6xHis tag from the recombinant protein at the concentration of 1mg/ml. The reactions were performed at 4°C under continuous rocking. The protein samples (36 µl) were taken at various times (0, 1, 2, 18, and 24 hours). The samples were centrifuged to remove the resin, and the supernatants were analyzed for cleavage efficiency using SDS-PAGE. After 24 hours of digestion, most of the tag less protein was collected in a tube and 0.1x Protease Inhibitor Cocktail (Sigma-Aldrich Cat. no. S88340) was added to quench the digestion reaction. The tag less protein was concentrated using Vivaspin 6 MWCO 10k concentrator (Cytiva Cat. no. 28932296).

1.2.6. Autodock

AutoDock was used to dock Nobiletin into the hRORγ protein (PDB: 5k38) providing the best binding position and orientation [37].

1.3. RESULTS

1.3.1. Expression and purification of hRORγ

The recombinant protein hRORγ was successfully induced and expressed reproducibly in *E. coli* (Figure 5). The affinity column (5ml) sequestered all the soluble recombinant hRORγ from the expression of 20L culture. Most of the contaminants were eliminated by washing the column with the buffer that has 60mM imidazole. Relatively pure recombinant protein was obtained in the elution using the buffer that has 200mM imidazole (Figure 6). The eluted recombinant hRORγ protein was immediately desalted to remove imidazole (Figure 7).

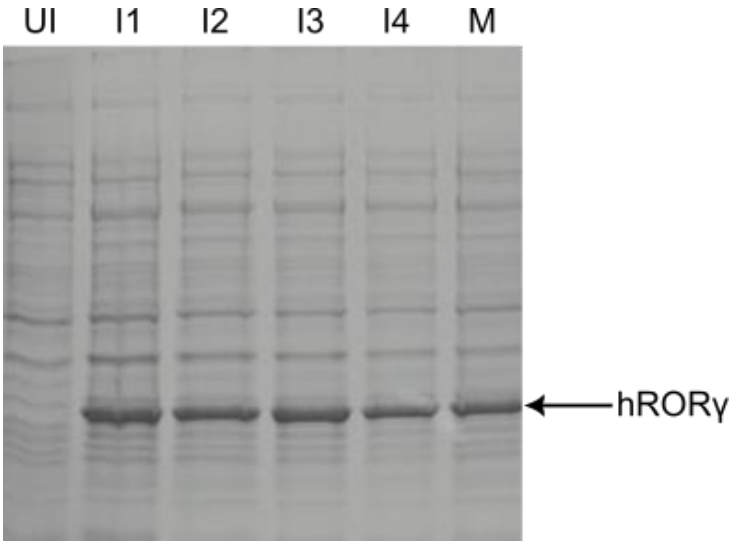

Figure 5: SDS-PAGE of hRORγ expression. Lanes 1-6 are uninduced (UI), four induced (I1, I2, I3, I4), and previously expressed (M) samples, respectively. The arrow on the right points to the induced band of hRORγ with expected molecular weight of ~31kDa.

(A)

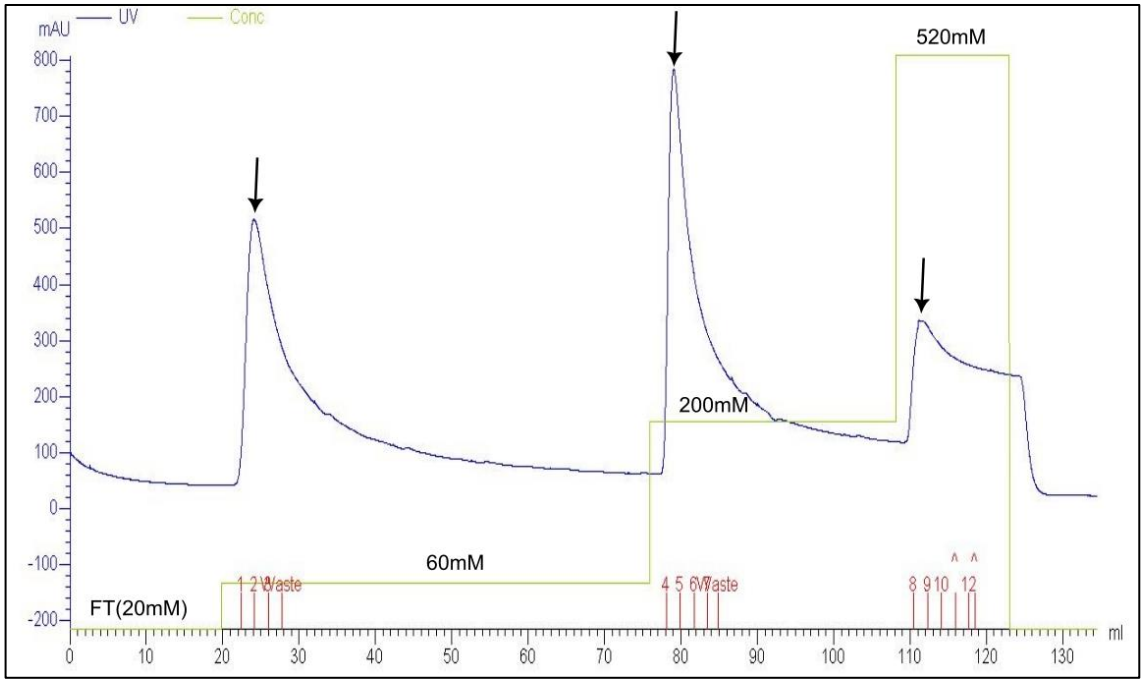

(B)

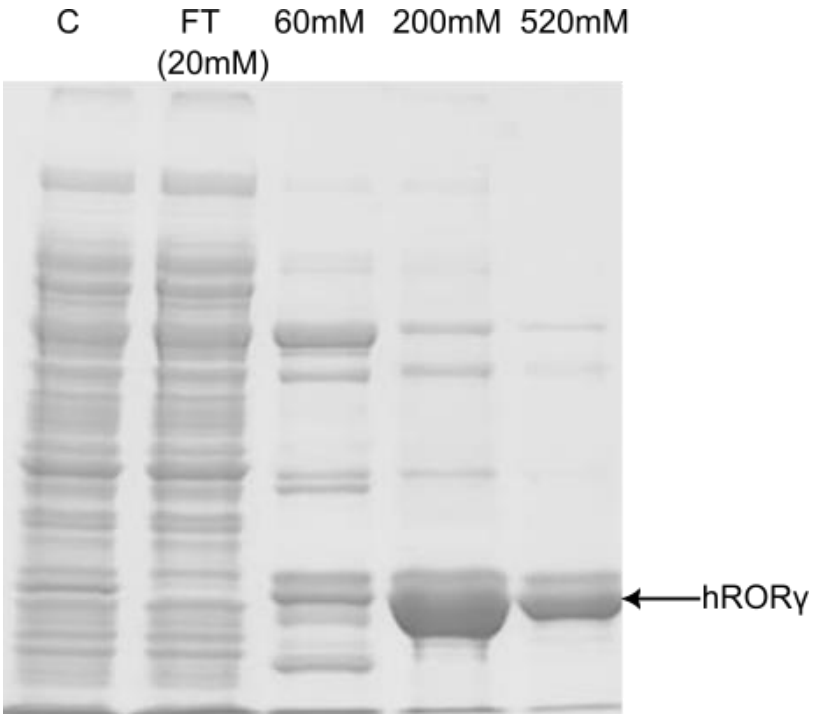

Figure 6: Affinity purification of hRORγ. (A) Chromatogram. The blue curve is UV_{280} absorbance (Y-axis) vs volume (X-axis). The green line is an imidazole step gradient with corresponding concentration labeled above. Samples were collected for the three peaks (black vertical arrows) with fractions indicated by the red vertical lines on the X-axis. **(B)** SDS-PAGE. Lanes 1-5 are Crude (C), Flow-through (FT), and step gradient samples (60mM, 200mM and 520mM), respectively. The black arrow on the right points to the hRORγ bands with expected molecular weights of ~31kDa.

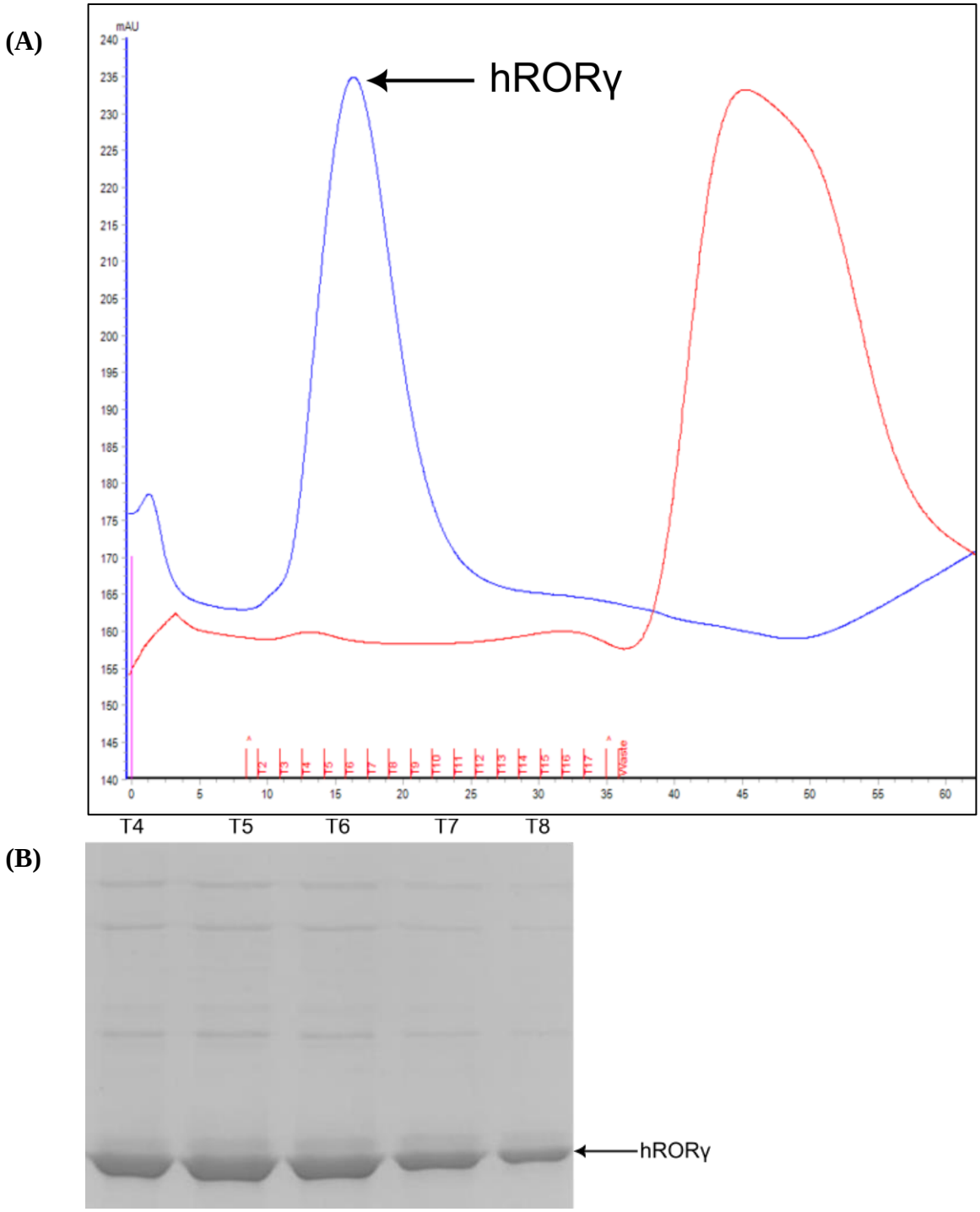

Figure 7: Desalting of affinity purified recombinant hRORγ. (A) Chromatogram. The blue curve is UV_{280} absorbance (Y-axis) vs fractions volume (X-axis). The red curve indicates the salt concentration. Samples were collected for the peak of the blue curve (black horizontal arrow) with fractions indicated by the red vertical lines and tube number on the X-axis. **(B)** SDS-PAGE. Lanes 1-5 are collected fractions T4, T5, T6, T7 and T8 from panel **(A)**, respectively. The black arrow on the right points to the hRORγ bands with expected molecular weights of ~31kDa.

1.3.2. Thrombin digestion and concentrating recombinant hRORγ

To remove his-tag, the desalting hRORγ samples were digested with thrombin for 1, 2, 18, and 24hours. The digestion products were analyzed using SDS-PAGE. The digestion product slightly increased with longer digestion times. The results showed an increase in digestion product over time and completed digestion after 24 hours (Figure 8A). The tag less hRORγ were concentrated using ultrafiltration (Figure 8B).

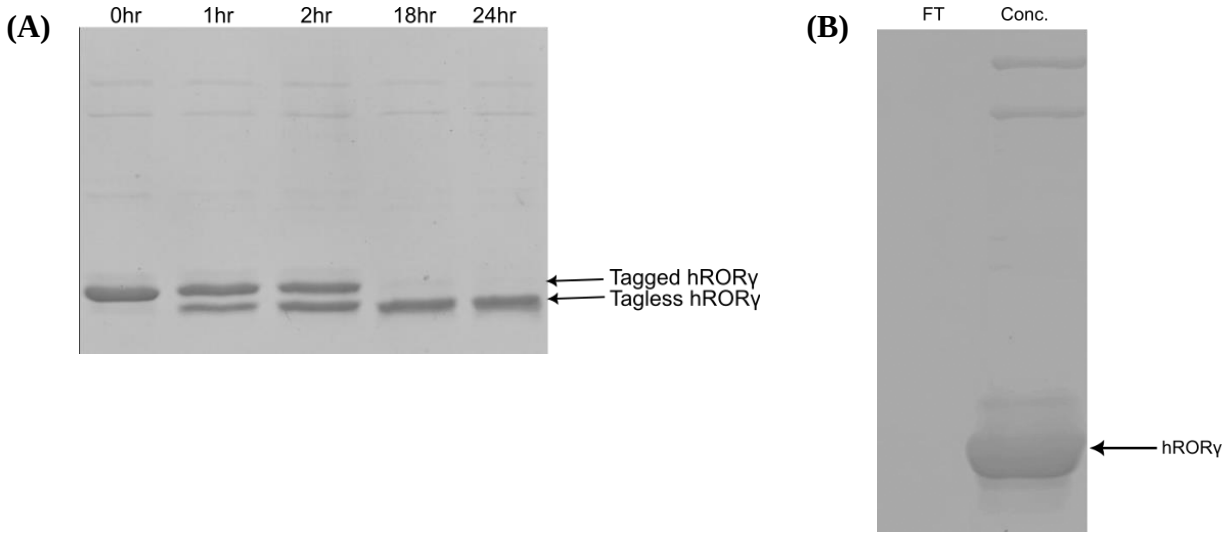

Figure 8: Thrombin digestion and concentrating of hRORγ. (A) SDS-PAGE of thrombin digestion. Lanes 1-5 are digested samples collected at 0, 1, 2, 18, and 24 hours, respectively. The two arrows on the right point to the tagged and tag less hRORγ, respectively. **(B)** SDS-PAGE of concentrated hRORγ. Samples were concentrated from panel **(A)** (lane 5). Lanes 1 and 2 were flow-through (FT) and concentrated (Conc.) hRORγ, respectively. The arrow on the right points to the tag less hRORγ band with expected molecular weights of ~30kDa.

1.3.3. Protein-ligand binding prediction

This study used AutoDock Vina, a software that utilizes biophysics techniques to simulate the interaction between hRORγ-Nobiletin binding. It predicted their binding modes and affinities. The hRORγ-Nobiletin can bind four different modes with affinities (Table 1). However, it is important to verify the results obtained through this method with wet lab experiments.

Table 1:hRORγ-Nobiletin docking binding mode and affinity

Binding Mode	Binding affinity
1	-7.8
2	-7.5
3	-7.4
4	-7.4

(A) **(B)**

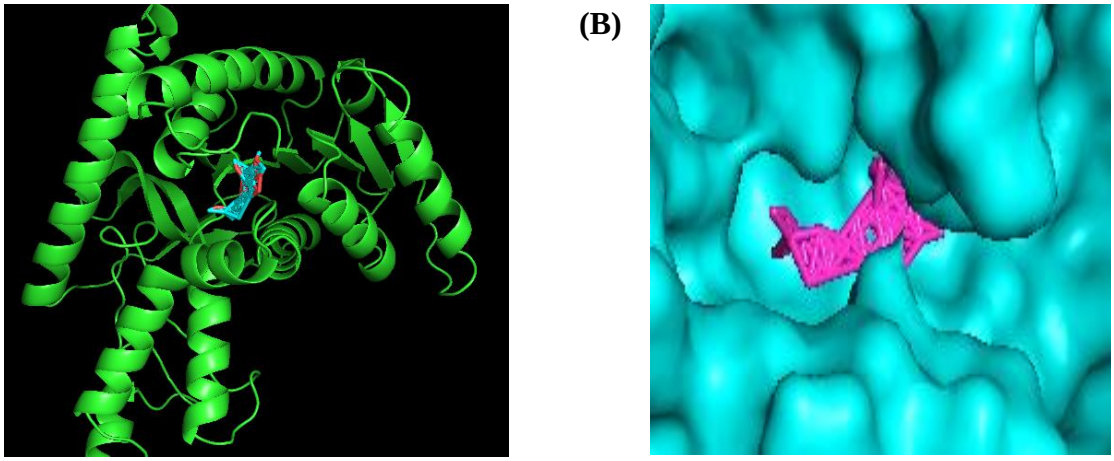

Figure 9: hRORγ-Nobiletin binding prediction by using Autodock vina software and visualized by Pymol. (A) Ribbon diagram of hRORγ (green)-Nobiletin (cyan) complex. **(B)** Close view of hRORγ (cyan) -Nobiletin (magenta) complex binding interaction [37, 38].

1.4. DISCUSSION

The thrombin digestion of hRORγ is a crucial step before co-crystallization experiments with Nobiletin. The optimization of thrombin digestion is a critical factor in obtaining a protein sample suitable for co-crystallization. Achieving high protein concentration is vital for obtaining clear and well-diffracting crystals, which are needed for structural studies. This strategy aligns with the goal of obtaining accurate structural insights into the hRORγ-Nobiletin complex. Although the progress achieved in protein expression, purification and thrombin digestion, additional work is required to fine-tune protocol. The goal is to enhance the efficiency of digestion while minimizing any potential protein degradation. Additionally, careful consideration should be given to ensuring that the removal of the histidine tag does not compromise protein stability or

alter its conformation. Moving forward, several avenues of research can be explored to optimize thrombin digestion and advance the co-crystallization process. Continue to systematically refine the thrombin digestion conditions, exploring different digestion times, enzyme-to-substrate ratios, and buffer compositions. Monitoring the digestion progress through gel electrophoresis and analytical techniques will be valuable in assessing the quality of the digestion process. Evaluate the stability of the histidine tag-free hRORγ protein by conducting thermal stability assays and assessing its secondary and tertiary structure. This will provide insights into whether the absence of the tag affects protein stability. Beyond structural insights, conduct functional assays to understand the biological implications of the hRORγ-Nobiletin interaction. Investigate how Nobiletin binding may impact hRORγ transcriptional activity and its potential implications for drug development.

In conclusion, the successful expression, purification, and thrombin digestion of hRORγ and the ongoing efforts to optimize thrombin digestion represent significant progress in the pursuit of co-crystallizing hRORγ with Nobiletin. Through careful refinement of experimental procedures and a comprehensive exploration of binding interactions, this research has the potential to contribute valuable insights to both structural biology and drug discovery.

1.5. FUTURE WORK

The future direction of this research will focus on refining several critical aspects of the study. The histidine-tag-free hRORγ protein's structural integrity will be extensively assessed to ensure its suitability for further investigation. In addition, the optimization of crystallization conditions will be a parallel effort involving various reagents to promote high-quality crystal growth. In the upcoming research, the hRORγ complex with Nobiletin compound will be crystallized at 20°C using the hanging drop method. This requires mixing a protein solution

(10mg/ml) with 0.2M ammonium sulfate, 0.1M Bis–Tris at pH 6.5, and 14% (w/v) polyethylene glycol 8000 based on previously published crystallization conditions [39]. After crystallization, the crystals will be rapidly transferred to a reservoir with 20% (v/v) glycerol and flash-frozen in liquid nitrogen. The X-ray diffraction data will be collected at the synchrotron radiation source, such as European Synchrotron Radiation Facility (ESRF), Advanced Photon Source (APS), National Synchrotron Light Source II, etc. Pursuing multiple crystallization conditions will increase the chances of obtaining crystals that are suitable for a detailed structural analysis.

Chapter 2: Purification of Vp54 from the PBCV-1 virus

2.1. INTRODUCTION

Giant viruses are exceptionally large viruses with diameters ranging from 200 to 2,000 nanometers, some of which surpass the size of typical bacteria[40, 41]. These viruses are recently classified within the new phylum Nucleocytoviricota (NCVs) originally grouped as Nucleocytoplasmic large DNA viruses[42]. They possess extensive double-stranded DNA genomes, ranging from 300 to over 1000 kilobase pairs, and these genomes encode a substantial number of genes, usually around 1000 genes[42, 43].

In the past four decades, a significant number of large double-stranded DNA (dsDNA) icosahedral viruses have been identified and categorized within the (NCVs) group. One of the initial NCVs discovered is the Paramecium Bursaria Chlorella virus type 1 (PBCV-1). It was first identified in 1981 by Russel H. Meints, James L. van Etten, etc among several other Chloroviruses. These viruses were initially named HVCV (Hydra viridis Chlorella virus) because it was observed infecting Chlorella-like algae[44, 45]. PBCV-1 is a large double-stranded DNA virus with a linear genome of approximately 331kb, predicted to encode around 416 proteins. Its genome is enclosed in an internal single bilayered lipid membrane, surrounded by an icosahedral outer capsid assembled from the major capsid protein (MCP) (Figure 10) [46, 47] .

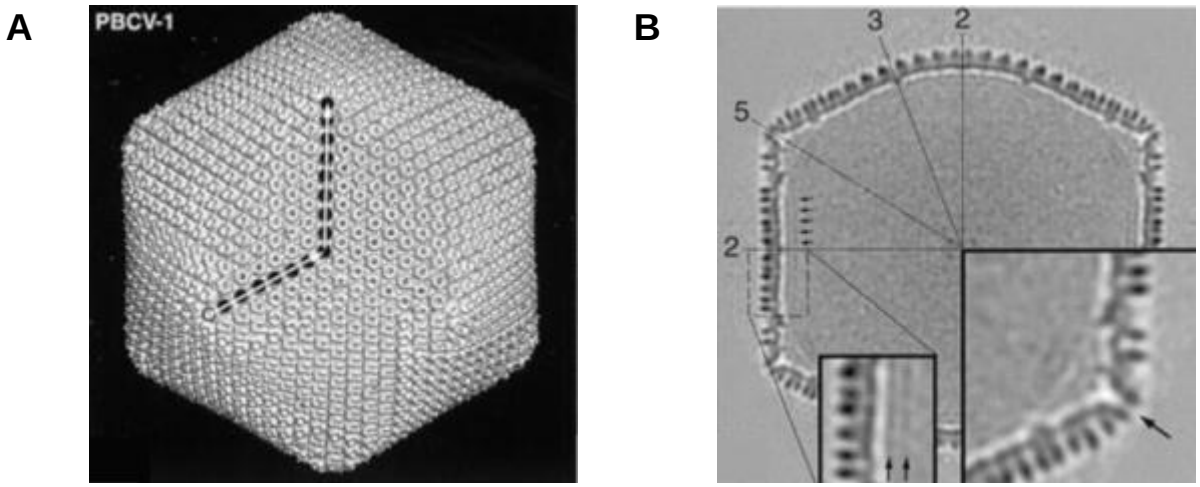

Figure 10: The structure of PBCV-1 virus. (A) Shaded-surface representations of the three-dimensional reconstructions of PBCV-1, each viewed down an icosahedral three-fold axis. **(B)** Central sections of the reconstruction density maps as viewed along a two-fold axis. A lipid bilayer exists beneath the capsid shell in virions (black arrows). This figure is adapted from Yan, X., et al., 2000 [47].

2.1.1. The PBCV-1 major capsid protein, Vp54 structure

Capsid of PBCV-1 is made up of pseudohexagonal arrays of donut-shaped capsomers, building block of the viral capsid (Figure 11) [46]. Each capsomer is composed of three molecules of glycoprotein, Vp54, the MCP of PBCV-1. Vp54 has been purified from the virus and crystallized. The X-ray crystallographer has determined its atomic structure to a resolution of 2.0Å [46]. The Vp54 trimer has a diameter of 72Å and a thickness of ≈75Å. Each monomer of Vp54 consisted of a 437 amino acid polypeptide chain with some surface residue glycosylated (Figure 12A). The monomeric of Vp54 polypeptide is composed of two consecutive domains D1 and D2. The first domain, D1, spans from residues 27 to 212, while the second domain, D2, spans from residues 225 to 437 (Figure 12A). Each of these domains has a structural motif known as jelly-roll fold. The jelly-roll fold is the β- sandwich that consists of two antiparallel β-sheets [48]. After the atomic structure of Vp54 was determined, the intact capsids of PBCV-1 were studied by electron microscopy first at 26Å resolution and later gradually improved to the near-atomic resolution of

3.5Å [47, 49, 50]. The atomic structure Vp54 has been fit into the Cry EM map to understand the overall capsids structure [46].

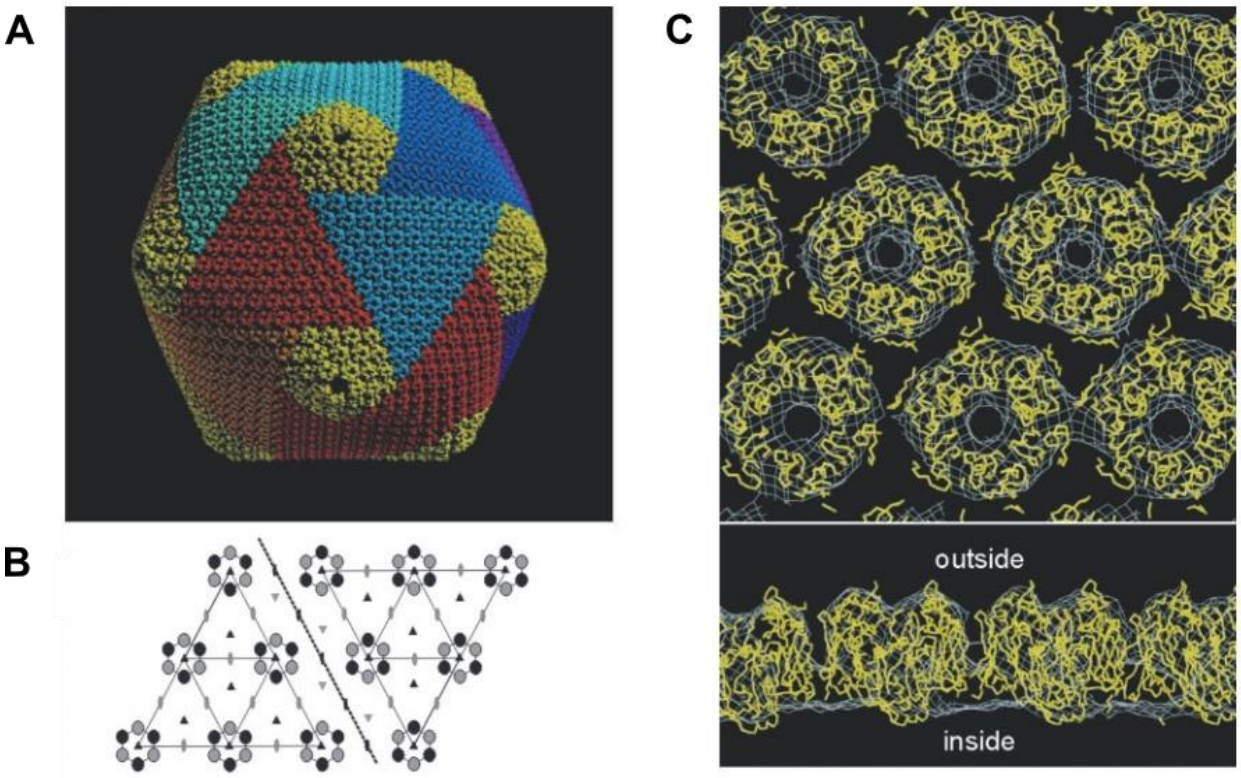

Figure 11: (A) Quasi-atomic model of the PBCV-1 capsid of the Vp54 trimer in the cryo-EM reconstruction. The pentasymmetrons are yellow colored to distinguish them from the trisymmetrons. **(B)** The symmetry elements in the PBCV-1 trisymmetron are illustrated. The black color denotes the p3 symmetry elements and the gray color represents the pseudo-p6 symmetry elements. **(C)** PBCV-1 Vp54 trimers located near the center of a trisymmetron are fitted into a cryo-EM map (white) and viewed from outside the virus (top) and from the side (bottom). This figure is adapted from Nandhagopal, N., et al., 2002 [46].

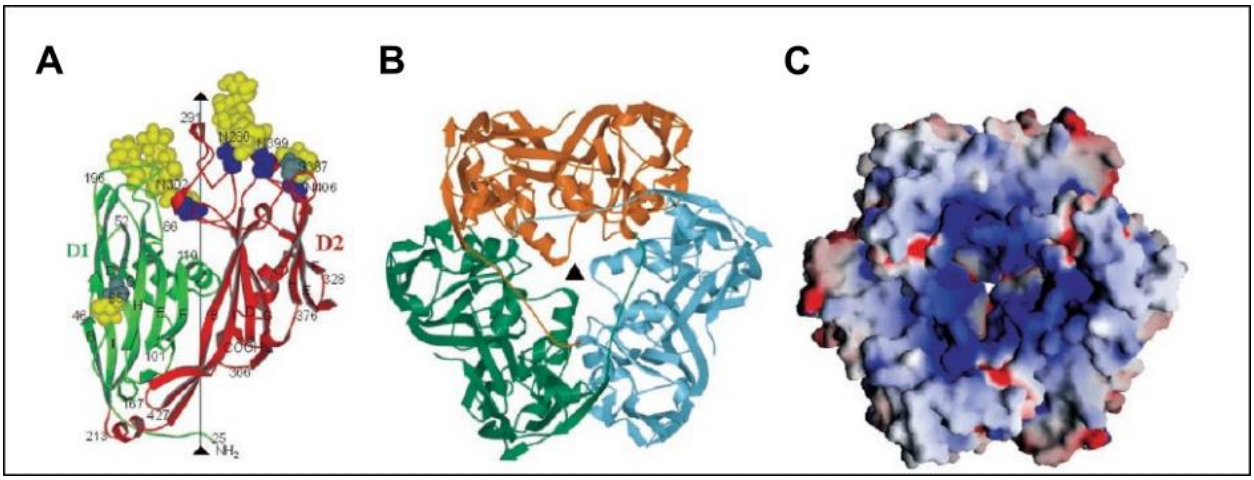

Figure 12: The structure of PBCV-1 major capsid protein, Vp54. (A) The structure of the Vp54 monomer is shown with specific amino acids labeled, yellow carbohydrate moieties, and Asn and Ser amino acids in blue and gray, respectively. **(B)** The VP54 trimer is shown from the virus's interior, with each monomer colored differently. **(C)** The Vp54 trimer surface, viewed from inside the virus, is color-coded by charge distribution. This figure is adapted from Cherrier, M.V., et al., 2009 [48].

2.1.2. Lipid analyses

Lipids play a crucial role in forming bilayer membranes, ensuring the fluidity and selective permeability of cell membranes [51]. The structural diversity of lipids, which can be derived from basic building blocks such as ketoacyl and isoprene groups, is estimated to exceed 200,000, with various molecular species combinations [52]. Lipidomic research aims to identify and quantify the entire profile of lipid molecules in cells, tissues, or organisms [52, 53]. Due to the large variation of lipid molecules, the lipidomic studies heavily rely on mass spectrometry (MS), an analytical technique that allows the study of intact lipid species in both quantitative aspects (concentration or molecular mass) and qualitative aspects (structure) [54].

The study of lipids has been extensively investigated in animals, plants, fungi, and bacteria, but it remains relatively understudied in microalgal cells [55]. Phospholipids (PL) constitute about 10-20% of the total lipids found in algal membranes. These consist of phosphatidylcholine (PC), phosphatidylglycerol (PG), phosphatidylethanolamine (PE),

phosphatidylinositol (PI), phosphatidylserine (PS), and phosphatidic acid (PA) [56]. Algal membranes also contain glycolipids such as monogalactosyldiacylglycerol (MGDG), digalactosyldiacylglycerol (DGDG), and sulfoquinovosyldiacylglycerol (SQDG), diacylglycerol (DAG) and triacylglycerol (TAG). Cardiolipin (CL), also known as diphosphatidylglycerol, is found mostly in the inner mitochondrial membrane. CL is a key phospholipid in mitochondrial bioenergetics and triggers programmed cell death of host cells [57].

2.1.3. Goals

Lipids are vital components within many viruses, primarily constituting viral membranes. In this study, we focus on isolating and purifying the major capsid protein Vp54 from the PBCV-1. In addition, we also focus on identifying the lipid components in the viral membrane and investigating the interactions between these lipids and the major capsid protein. To better understand how these lipids affect the assembly, stability, or other functions of the virus, it is important to study their association with Vp54.This evaluation will shed light on the role of lipids in viral replication. This research will contribute to a better knowledge of the virus's structure and function, as well as its potential applications in various fields such as virology and biotechnology.

2.2. METHODS AND MATERIALS

2.2.1. Prepare a lysate sample

The milky PBCV-1 virus sample (8mg/ml) is resuspended and aliquoted into 1ml per 1.5ml Eppendorf tube. The aliquoted PBCV-1 samples were heated at 70°C using water bath (Fisher Scientific Isotemp 6200 R35) for 30 minutes until Vp54 trimers were solubilized. The insoluble material was removed by centrifugation at 15,000xg for 20 minutes. After centrifugation, the supernatant and the pellet were separated. The pellet was immediately flash frozen using liquid

nitrogen for lipid analyses later. The supernatant samples were then filtered using a 0.2µm membranes filter (Fisher scientific Cat. no. 88520).

2.2.2. Purification of PBCV-1 Vp54

2.2.2.1. Cation- and anion-exchange column Chromatography

AKTA Pure (Cytiva) was used for the ion-exchange chromatography of PBCV-1 Vp54. The cation-exchange column (1ml) Hitrap SP XL (GE Cat. no. 17516001) and the anion-exchange column (1ml) Hitrap DEAD ff (GE Cat. no. 17505501) were tried to purify Vp54. Before loading the supernatant samples, the column was equilibrated with filtered and degassed Buffer A (50mM Tris-HCl, 10mM $MgCl_2$, and pH 7.8) for at least 5 column volume or until the UV baseline. The supernatant with Vp54 was then loaded onto the column at a flow rate of 1ml/min. Trial purifications were performed to elute the Vp54 protein using a linear gradient step from 0 to 100% with high salt Buffer B (50mM Tris–HCl, 1M NaCl, 10mM $MgCl_2$ and pH 7.8). Throughout the purification process, protein fractions were collected, and their purity was evaluated using SDS-PAGE. The molecular weight of Vp54 was ~54kDa. The comparison between cation and anion exchange chromatography were evaluated (Figure 17).

2.2.2.2. The large -scale cation-exchange chromatography

After comparing cation- and anion-exchange chromatography using 1ml column, purer Vp54 was found using the former one. Therefore, the protocol for purification Vp54 was updated using 53ml HiLoad 26/10 SP Sepharose column (GE Cat. no. 17113801). Prior to loading samples, the column was equilibrated with filtered and degassed Buffer A (50mM Tris-HCL, 10mM $MgCl_2$, and pH 7.8) for at least 5 column volume or until the UV reaches the baseline. The supernatant samples were then loaded onto the column at a flow rate of 8ml/min. The purification was performed to elute the Vp54 protein using a linear gradient step from 0 to 100% with high salt Buffer B (50mM Tris–HCl, 1M NaCl, 10mM $MgCl_2$ and pH 7.8). Throughout the purification

process, fractions were collected and analyzed using SDS-PAGE to assess the purity and yield of Vp54. The collected samples were concentrated, and buffer exchanged to sodium phosphate buffer (50mM Na_3PO_4, 100mM NaCl, and pH 7) using a Vivaspin 20 MWCO 30k concentrator (Cytiva Cat. no. 28932358).

2.2.3. MS/MS spectrometry and liposome co-sedimentation assay

MS/MS spectrometry and liposome co-sedimentation assay was carried out by Dr. Denial's group using their established protocols.

2.3. RESULTS

2.3.1. Sample preparation and purification

The Vp54 samples were successfully separated from PBCV-1 virus. The pellet and the supernatant samples were evaluated on SDS-PAGE (Figure 13). During the cation- and anion-exchange purification trials, the Vp54 was not bound to the column, but eluted out in the flow through. Although it was not bound to the column, the flow through sample was relatively pure. The Vp54 protein was collected from both cation- and anion-exchange chromatography and its purity was compared using SDS-PAGE. (Figure 17).

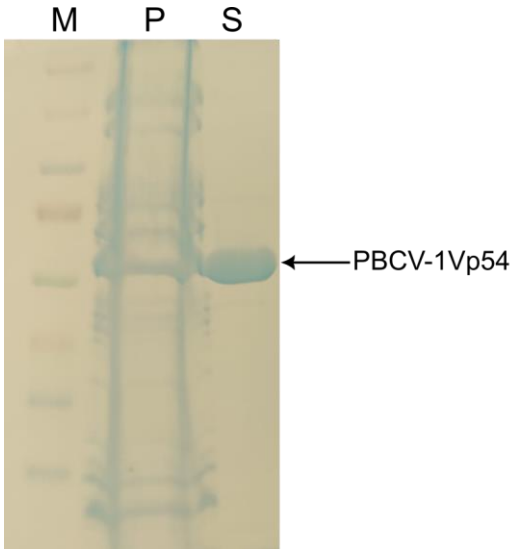

Figure 13: SDS-PAGE of PBCV-1 Vp54. Lanes 1-3 are Molecular weight marker (M), Pellets (P), and Supernatant (S), respectively. The black arrow on the right points to the PBCV-1 Vp54 bands with expected molecular weights of ~54kDa.

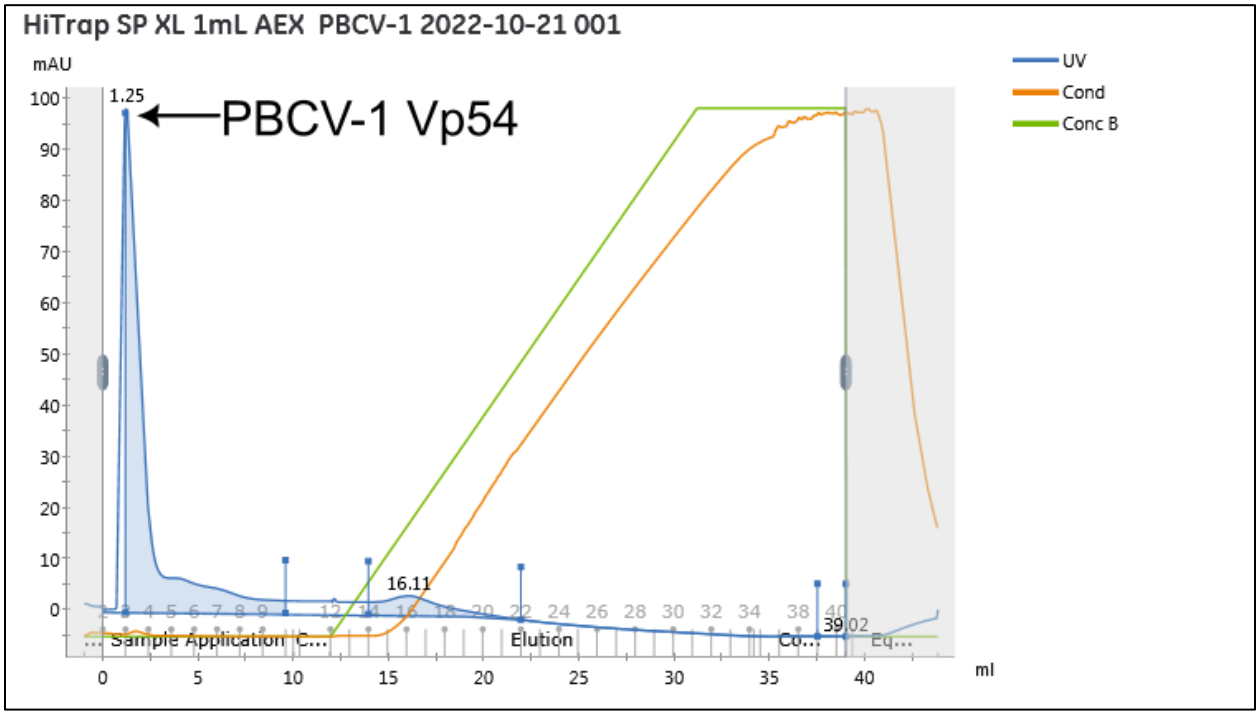

Figure 14: Cation-exchange chromatography of PBCV-1 Vp54. The blue curve is UV_{280} absorbance (Y-axis) vs elution volume (X-axis). The brown line and green line are conductivity and gradient concentration (0 to 100%), respectively. Samples were collected for the peak (black horizontal arrow) with fractions indicated on the X-axis. The black arrow points to the PBCV-1 Vp54 peak.

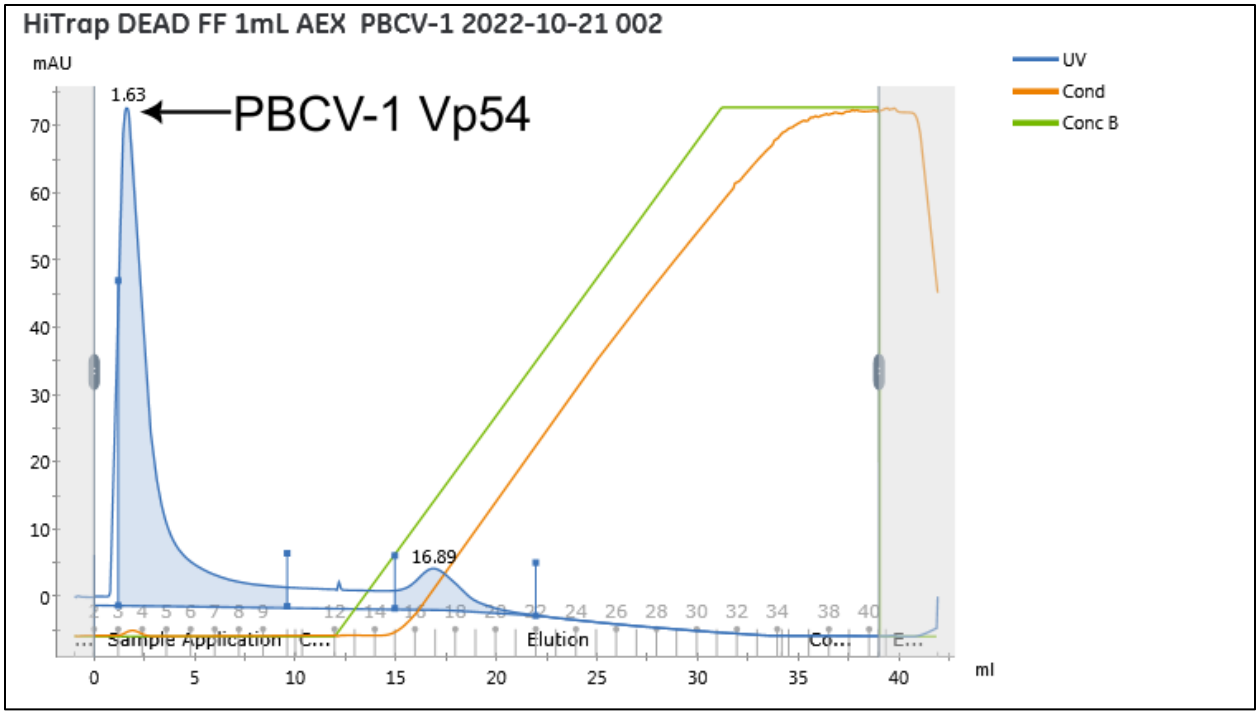

Figure 15: Anion-exchange chromatography of PBCV-1 Vp54. The blue curve is UV_{280} absorbance (Y-axis) vs elution volume (X-axis). The brown line and green line are conductivity and gradient concentration (0 to 100%), respectively. Samples were collected for the peak (black horizontal arrow) with fractions indicated on the X-axis. The black arrow points to PBCV-1 Vp54 peak.

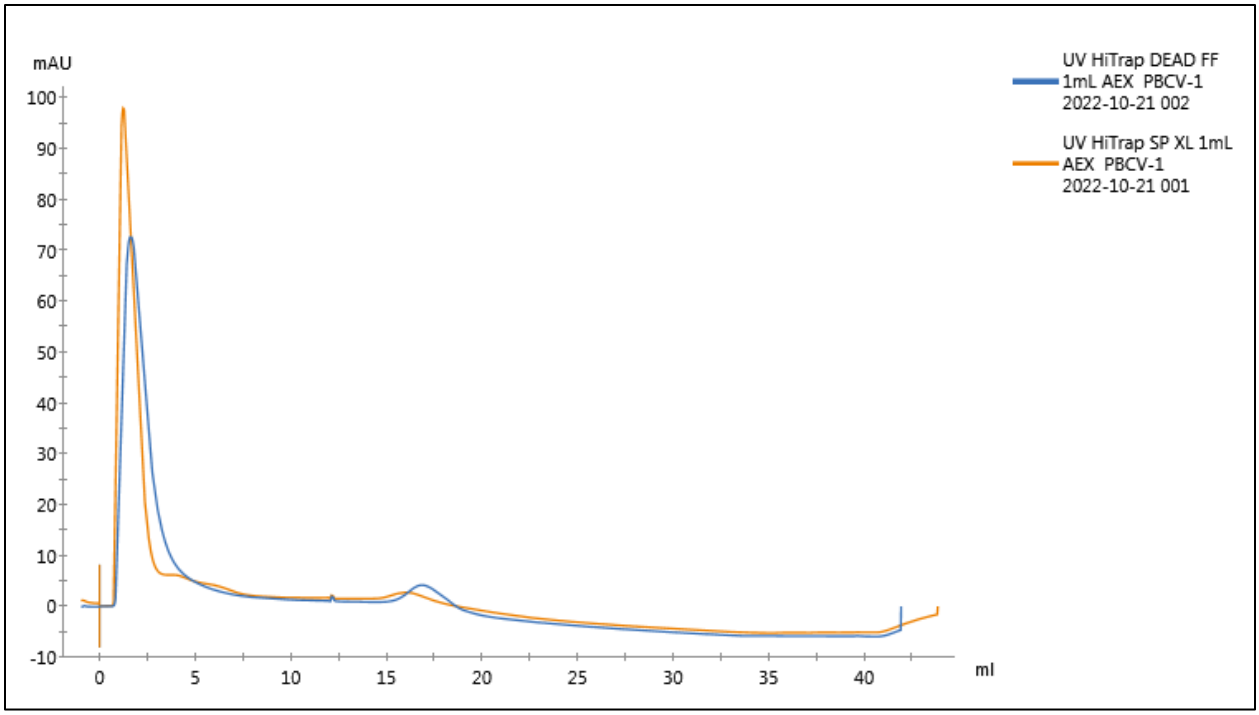

Figure 16: Comparison between cation- and anion-exchange chromatography. The orange line and blue line indicated cation- and anion-exchange chromatography. The purify sample from cation- and anion-exchange chromatography were evaluated using SDS-PAGE (Figure 17).

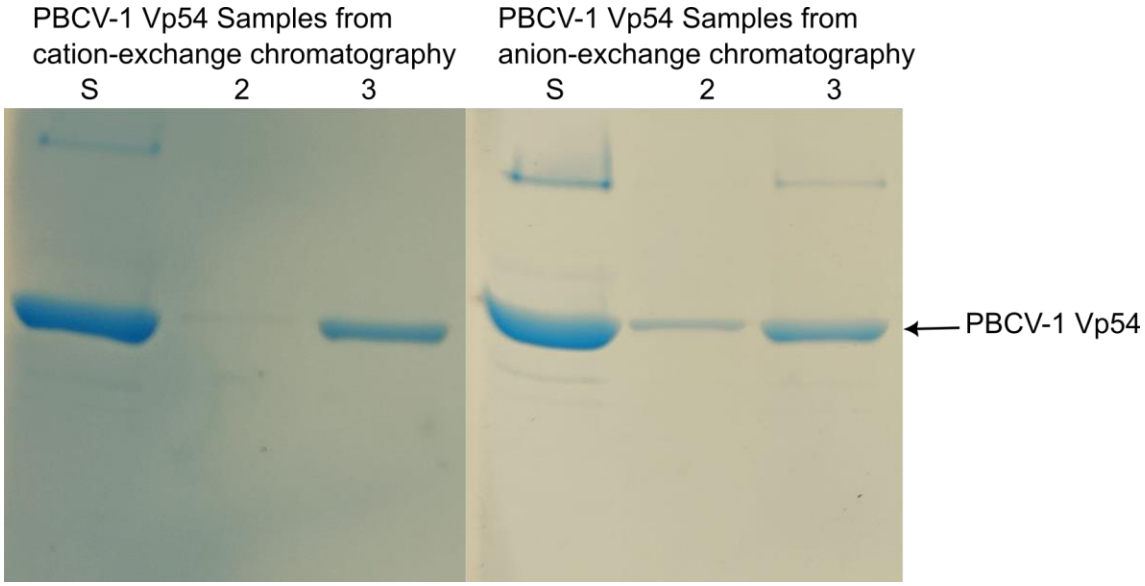

Figure 17: SDS-PAGE of cation- and anion-exchange chromatography. The left to right side of the gels were collected from cation- and anion-exchange chromatography, respectively. For each of the cation-and anion-exchange chromatography, Lanes 1-3 are Supernatant (S), 2, and 3 samples from chromatogram, respectively. The black arrow on the right points to the PBCV-1 Vp54 bands with expected molecular weights of ~54kDa.

2.3.1.1. The large-scale Cation-exchange chromatography and concentrating of PBCV-1 Vp54

Three peaks were successfully separated through large-scale cation-exchange chromatography (Figure 18). The first peak consisted of flow-through samples that were not bound to the column. The second and third peaks were samples that eluted from the gradient. After the Vp54 was purified on a large scale, The first and second peak samples were concentrated and underwent buffer exchange to phosphate buffer. They were labeled as C1 and C2 respectively. The concentration of Vp54 in both C1 and C2 was about 4mg/ml and 4.6mg/ml, respectively (Figure 19).

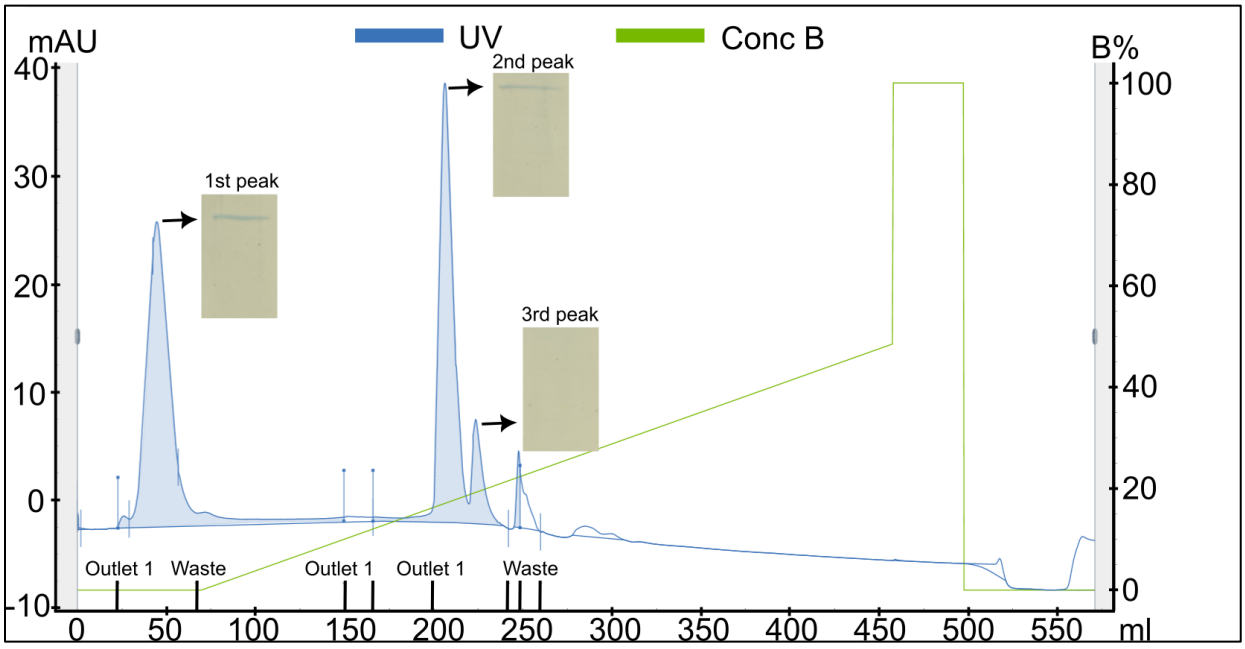

Figure 18: Cation-exchange chromatography of PBCV-1 Vp54. The blue curve is UV_{280} absorbance (Y-axis) vs elution volume (X-axis). The green line was gradient concentration (0 to 100%) (after 50% step up to 100%). The black arrows link correspondent peaks with their SDS-PAGEs, respectively.

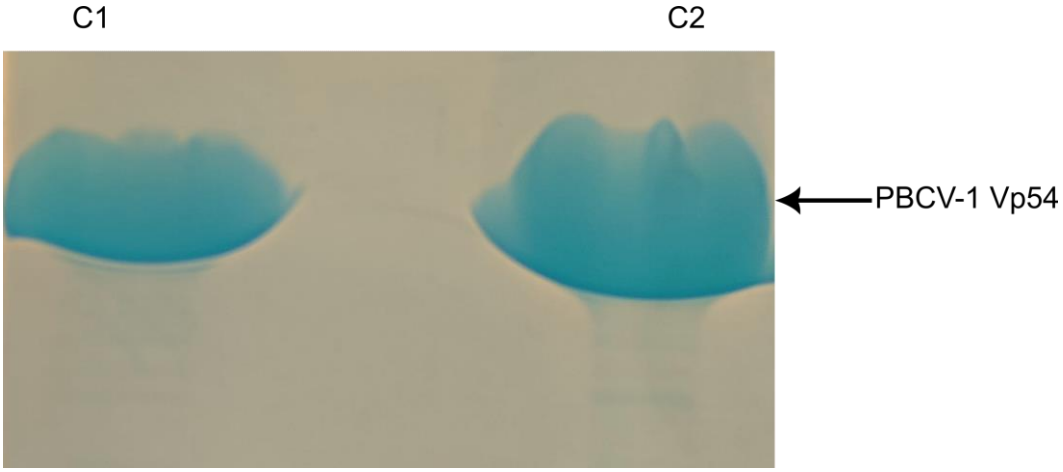

Figure 19: SDS-PAGE of concentrated PBCV-1 Vp54 samples. The black arrow on the right points indicated the expected molecular weight of Vp54 is ~54kDa.

2.3.2. Mass spectrometry

Dr. Daniel's group found four lipid classes, including diacylglycerols, phosphatidylcholines, glycosyl-based lipids, and cardiolipins, using MS/MS spectrometry. The major constituents of the PC class were identified using the six highest intensity peaks, which showed the most abundance relevant to the PC class.

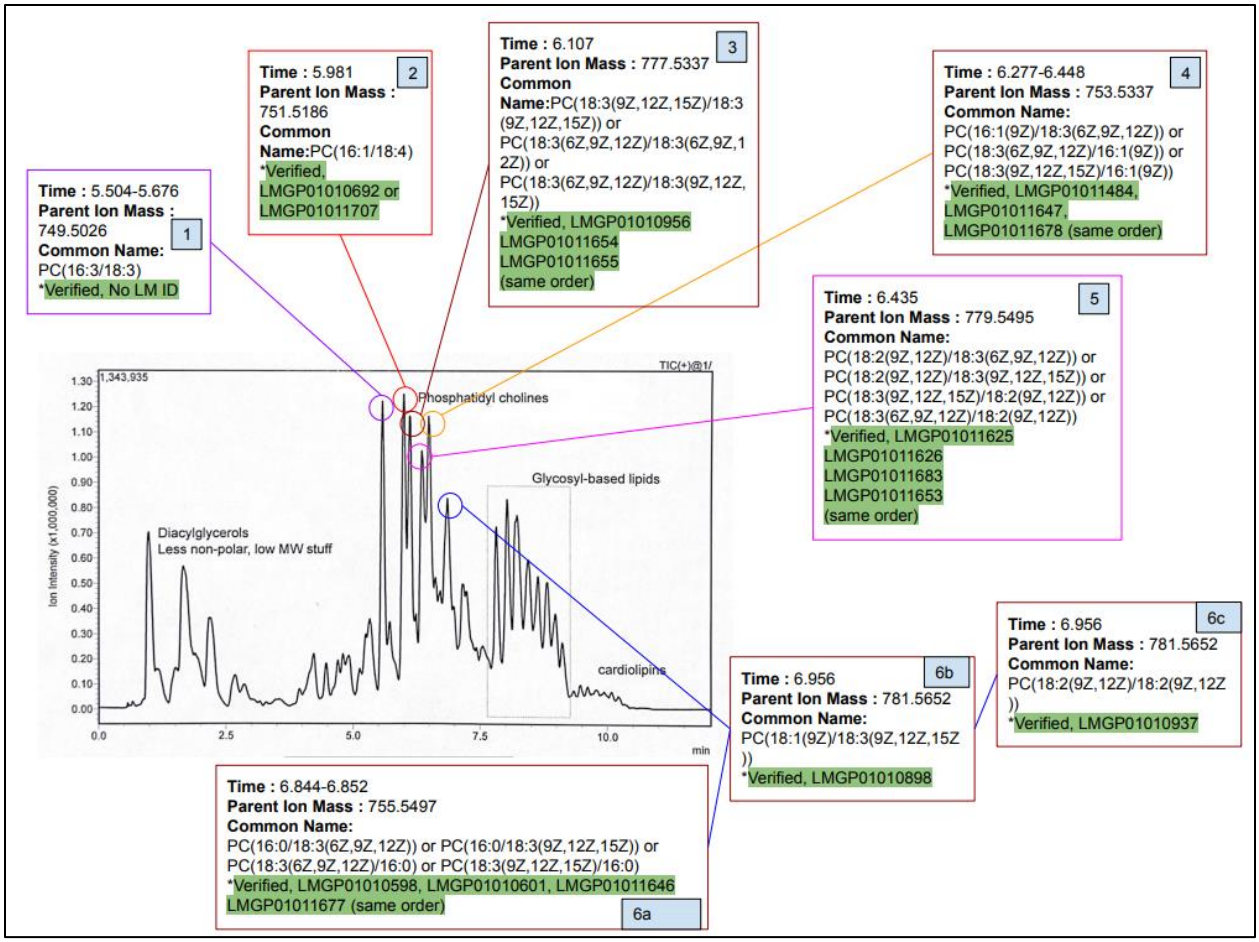

Figure 20: Four lipid classes were identified in the sample: Diacylglycerols, Phosphatidylcholines, Glycosyl-based lipids, and Cardiolipins. (Unpublished data from Dr. Daniel group)

2.3.3. Liposome co-sedimentation assay

Dr. Daniel's group also found that Vp54 preferentially bound to *in vitro* constituted liposomes with cardiolipin and other lipids (Figure 21A-C). Cytochrome C, another cardiolipin-binding protein, was used as a control to compare (Figure 21B-C). Liposomes containing PG serve as a precursor for cardiolipin synthesis and show weaker binding to Vp54 and cytochrome C. The strongest binding was observed with liposomes containing cardiolipin, followed by liposomes containing PG and PE. On the other hand, both Vp54 and cytochrome C show little or no binding

to liposomes containing PC. Dr. Daniel's group is continuing to test the bindings using a large amount of Vp54 purified from our group.

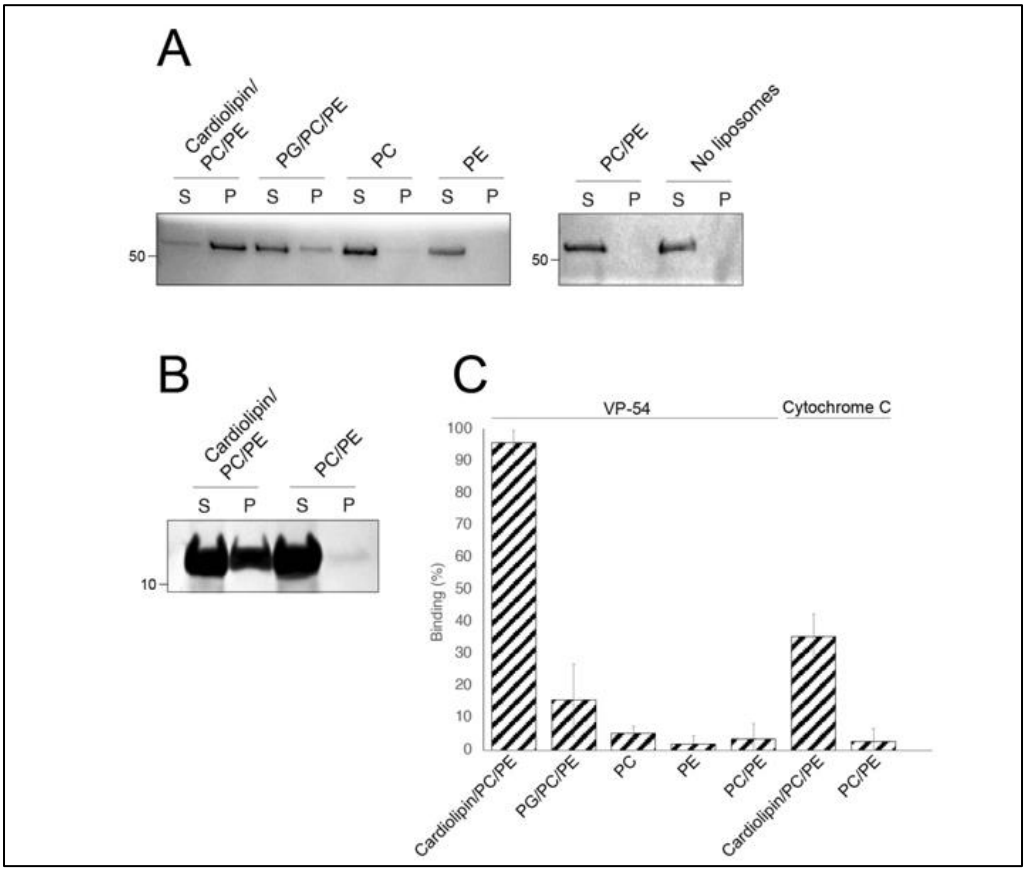

Figure 21: Binding of Vp54 to lipids. (A) Liposome sedimentation assay for Vp54 and cytochrome C **(B)** with the indicated lipid composition from figure 20. **(C)** Quantification of the binding of Vp54 and cytochrome C to liposomes with the indicated lipid composition. (Unpublished data from Dr. Daniel group).

2.4. DISCUSSION

Interestingly, Cardiolipin was detected in the PBCV-1 membrane by Dr. Daniel group. The presence of this mitochondrial phospholipid in the viral internal membrane suggests the possible sequestration of lipid membrane fragments from various other organelles during viral replication. This interaction between Vp54 and cardiolipin could impact numerous cellular processes, including membrane organization and cellular energetics, as well as viral replication or

assembly within host cells. This finding will potentially lead to a better insight of the replication of PBCV-1.

2.5. FUTURE WORK

In future research, the primary focus is on optimization of the ion-exchange purification process to achieve a higher concentration of viral protein, Vp54, without introducing contamination. An essential aspect of this research will facilitate the binding affinity studies of Vp54 to liposomes. Currently, there is not enough precise information regarding the affinity of these interactions. To address this, binding studies, and affinity assays such as Surface Plasmon Resonance (SPR) will be conducted to quantify the strength of the Vp54-lipid interactions. However, it is necessary to continue and repeat experimentation to obtain pure Vp54 and affinity assays for better understanding of their interaction.

References

1. Dunlap, J.C., *Molecular bases for circadian clocks.* Cell, 1999. **96**(2): p. 271-290.
2. Lowrey, P.L. and J.S. Takahashi, *Genetics of circadian rhythms in Mammalian model organisms.* Advances in genetics, 2011. **74**: p. 175-230.
3. Álamo, C. and F. López-Muñoz, *12 Chronobiological Rhythms, Melatonergic System, and Depression.* Neurobiology of Depression, 2011: p. 247.
4. Emery, P., et al., *Sensitive Timing: A Reappraisal of Chronobiology's Foundational Texts.* Journal of Biological Rhythms, 2023: p. 07487304231169080.
5. Sellers, L., *Rhythms of Life: The Biological Clocks That Control the Daily Lives of Every Living Thing.* Journal of College Science Teaching, 2006. **35**(5): p. 57.
6. Huang, R.-C., *The discoveries of molecular mechanisms for the circadian rhythm: The 2017 Nobel Prize in Physiology or Medicine.* Biomedical journal, 2018. **41**(1): p. 5-8.
7. Kreitzman, L. and R. Foster, *The rhythms of life: The biological clocks that control the daily lives of every living thing*. 2011: Profile books.
8. Wang, H., *Perfect timing: a Nobel Prize in Physiology or Medicine for circadian clocks.* Sci Bull, 2018. **63**(7): p. 398-401.
9. Piersimoni, L., et al., *Lighting up Nobel Prize-winning studies with protein intrinsic disorder.* Cellular and Molecular Life Sciences, 2022. **79**(8): p. 449.
10. Glossop, N.R.J., L.C. Lyons, and P.E. Hardin, *Interlocked feedback loops within the Drosophila circadian oscillator.* Science, 1999. **286**(5440): p. 766-768.
11. Wulund, L. and A.B. Reddy, *A brief history of circadian time: The emergence of redox oscillations as a novel component of biological rhythms.* Perspectives in Science, 2015. **6**: p. 27-37.
12. Wang, C., et al., *Interplay between Dioxin-mediated signaling and circadian clock: a possible determinant in metabolic homeostasis.* International journal of molecular sciences, 2014. **15**(7): p. 11700-11712.
13. Xue, T., et al., *Investigations of the CLOCK and BMAL1 proteins binding to DNA: a molecular dynamics simulation study.* PloS one, 2016. **11**(5): p. e0155105.
14. McIntosh, B.E., J.B. Hogenesch, and C.A. Bradfield, *Mammalian Per-Arnt-Sim proteins in environmental adaptation.* Annual review of physiology, 2010. **72**: p. 625-645.
15. Zhang, J., J.C. Chatham, and M.E. Young, *Circadian regulation of cardiac physiology: rhythms that keep the heart beating.* Annual review of physiology, 2020. **82**: p. 79-101.
16. Matsumura, R., et al., *The mammalian circadian clock protein period counteracts cryptochrome in phosphorylation dynamics of circadian locomotor output cycles kaput (CLOCK).* Journal of Biological Chemistry, 2014. **289**(46): p. 32064-32072.
17. Pevet, P. and E. Challet, *Melatonin: both master clock output and internal time-giver in the circadian clocks network.* Journal of Physiology-Paris, 2011. **105**(4-6): p. 170-182.
18. Schibler, U., *The mammalian circadian timekeeping system.* Ultradian rhythms from molecules to mind: a new vision of life, 2008: p. 261-279.
19. Pardee, K., A.S. Necakov, and H. Krause, *Nuclear receptors: small molecule sensors that coordinate growth, metabolism and reproduction.* A Handbook of Transcription Factors, 2011: p. 123-153.

20. Burris, T.P., S.A. Busby, and P.R. Griffin, *Targeting orphan nuclear receptors for treatment of metabolic diseases and autoimmunity.* Chemistry & biology, 2012. **19**(1): p. 51-59.
21. Zhang, Y., et al., *ROR nuclear receptors: structures, related diseases, and drug discovery.* Acta Pharmacologica Sinica, 2015. **36**(1): p. 71-87.
22. Solt, L.A. and T.P. Burris, *Action of RORs and their ligands in (patho) physiology.* Trends in Endocrinology & Metabolism, 2012. **23**(12): p. 619-627.
23. Preitner, N., et al., *The orphan nuclear receptor REV-ERBα controls circadian transcription within the positive limb of the mammalian circadian oscillator.* Cell, 2002. **110**(2): p. 251-260.
24. Mangelsdorf, D.J., et al., *The nuclear receptor superfamily: the second decade.* Cell, 1995. **83**(6): p. 835-839.
25. Giguere, V., et al., *Isoform-specific amino-terminal domains dictate DNA-binding properties of ROR alpha, a novel family of orphan hormone nuclear receptors.* Genes & development, 1994. **8**(5): p. 538-553.
26. Jetten, A.M., *Retinoid-related orphan receptors (RORs): critical roles in development, immunity, circadian rhythm, and cellular metabolism.* Nuclear receptor signaling, 2009. **7**(1): p. nrs-07003.
27. Jetten, A.M. and E. Ueda, *The ROR nuclear orphan receptor subfamily: critical regulators of multiple biological processes.* 2001.
28. Alam, M.N., M. Almoyad, and F. Huq, *Polyphenols in colorectal cancer: current state of knowledge including clinical trials and molecular mechanism of action.* BioMed research international, 2018. **2018**.
29. Lin, N., et al., *Novel anti-inflammatory actions of nobiletin, a citrus polymethoxy flavonoid, on human synovial fibroblasts and mouse macrophages.* Biochemical pharmacology, 2003. **65**(12): p. 2065-2071.
30. Seki, T., et al., *Nobiletin-rich Citrus reticulata peels, a kampo medicine for Alzheimer's disease: A case series.* Geriatrics & gerontology international, 2013. **13**(1): p. 236-238.
31. Huang, H., et al., *The multifunctional effects of nobiletin and its metabolites in vivo and in vitro.* Evidence-Based Complementary and Alternative Medicine, 2016. **2016**.
32. Tung, Y.-C., et al., *Polymethoxyflavones: chemistry and molecular mechanisms for cancer prevention and treatment.* Current Pharmacology Reports, 2019. **5**: p. 98-113.
33. Kesharwani, S.S., et al., *Nobiletin as a molecule for formulation development: an overview of advanced formulation and nanotechnology-based strategies of nobiletin.* Aaps Pharmscitech, 2020. **21**: p. 1-13.
34. Chen, Z., et al., *Identification of diverse modulators of central and peripheral circadian clocks by high-throughput chemical screening.* Proceedings of the National Academy of Sciences, 2012. **109**(1): p. 101-106.
35. He, B., et al., *The small molecule nobiletin targets the molecular oscillator to enhance circadian rhythms and protect against metabolic syndrome.* Cell metabolism, 2016. **23**(4): p. 610-621.
36. Cho, H., et al., *Regulation of circadian behaviour and metabolism by REV-ERB-α and REV-ERB-β.* Nature, 2012. **485**(7396): p. 123-127.
37. Forli, S., et al., *Computational protein–ligand docking and virtual drug screening with the AutoDock suite.* Nature protocols, 2016. **11**(5): p. 905-919.

38. Seeliger, D. and B.L. de Groot, *Ligand docking and binding site analysis with PyMOL and Autodock/Vina.* Journal of computer-aided molecular design, 2010. **24**(5): p. 417-422.
39. Wang, Y., et al., *Discovery of N-(4-aryl-5-aryloxy-thiazol-2-yl)-amides as potent RORγt inverse agonists.* Bioorganic & Medicinal Chemistry, 2015. **23**(17): p. 5293-5302.
40. Ogata, H., et al., *Remarkable sequence similarity between the dinoflagellate-infecting marine girus and the terrestrial pathogen African swine fever virus.* Virology Journal, 2009. **6**: p. 1-8.
41. Xiao, C., et al., *Cryo-EM reconstruction of the Cafeteria roenbergensis virus capsid suggests novel assembly pathway for giant viruses.* Scientific reports, 2017. **7**(1): p. 5484.
42. Van Etten, J.L., *Giant viruses.* 2011.
43. Legendre, M., et al., *Genomics of Megavirus and the elusive fourth domain of Life.* Communicative & integrative biology, 2012. **5**(1): p. 102-106.
44. Meints, R.H., et al., *Viral infection of the symbiotic chlorella-like alga present in Hydra viridis.* Virology, 1981. **113**(2): p. 698-703.
45. Hoshina, R., et al., *Isolation and characterization of a virus (CvV-BW1) that infects symbiotic algae of Paramecium bursaria in Lake Biwa, Japan.* Virology Journal, 2010. **7**(1): p. 1-10.
46. Nandhagopal, N., et al., *The structure and evolution of the major capsid protein of a large, lipid-containing DNA virus.* Proceedings of the National Academy of Sciences, 2002. **99**(23): p. 14758-14763.
47. Yan, X., et al., *Structure and assembly of large lipid-containing dsDNA viruses.* Nature structural biology, 2000. **7**(2): p. 101-103.
48. Cherrier, M.V., et al., *An icosahedral algal virus has a complex unique vertex decorated by a spike.* Proceedings of the National Academy of Sciences, 2009. **106**(27): p. 11085-11089.
49. Fang, Q., et al., *Near-atomic structure of a giant virus.* Nature communications, 2019. **10**(1): p. 388.
50. Shao, Q., et al., *Near-atomic, non-icosahedrally averaged structure of giant virus Paramecium bursaria chlorella virus 1.* Nature communications, 2022. **13**(1): p. 6476.
51. Van Meer, G., D.R. Voelker, and G.W. Feigenson, *Membrane lipids: where they are and how they behave.* Nature reviews Molecular cell biology, 2008. **9**(2): p. 112-124.
52. Seppänen-Laakso, T. and M. Orešič, *How to study lipidomes.* Journal of Molecular Endocrinology, 2009. **42**(3): p. 185-190.
53. Wenk, M.R., *The emerging field of lipidomics.* Nature reviews Drug discovery, 2005. **4**(7): p. 594-610.
54. Han, X. and R.W. Gross, *Shotgun lipidomics: electrospray ionization mass spectrometric analysis and quantitation of cellular lipidomes directly from crude extracts of biological samples.* Mass spectrometry reviews, 2005. **24**(3): p. 367-412.
55. Markham, J.E., et al., *Separation and identification of major plant sphingolipid classes from leaves.* Journal of Biological Chemistry, 2006. **281**(32): p. 22684-22694.
56. Kumari, P., et al., *Algal lipids, fatty acids and sterols*, in *Functional ingredients from algae for foods and nutraceuticals*. 2013, Elsevier. p. 87-134.
57. Paradies, G., et al., *Role of cardiolipin in mitochondrial function and dynamics in health and disease: molecular and pharmacological aspects.* Cells, 2019. **8**(7): p. 728.

Vita

Laila Noor received her bachelor's degree in Biochemistry and Molecular Biology from Jahangirnagar University in Bangladesh. After earning her bachelor's degree, Laila pursued a master's in chemistry at The University of Texas at El Paso. She was awarded the Summer Bridge to Doctorate Pilot Program in the summer of 2021. During the summer semester, she joined Dr. Xiao's structural biochemistry laboratory and worked on different projects. During her graduate studies, Laila worked as a Teaching and Research Assistant for the Chemistry and Biochemistry department. She has extensive experience in teaching General Chemistry, Organic Chemistry and Biochemistry lab courses. She also mentored undergraduate and graduate students in Dr. Xiao's lab. Moreover, she attended BioMolViz professional development training in Boston, Massachusetts, in 2022 and volunteered at the COURI Symposium to evaluate student presentations and their research projects.

Contact Information: lnoor@miners.utep.edu